

On Prolate Halos and Rotation Curves

K. Zatrimeylov

*Scuola Normale Superiore and INFN
Piazza dei Cavalieri 7, 56126, Pisa, Italy*

E-mail: kirill.zatrimeylov@sns.it

Abstract. We propose a simple geometrical mechanism for the flattening of galactic rotation curves, the local compression of field lines around their planes induced by elongated dark-matter halos, and elaborate on its possible role in Nature. Fitting 69 rotation curves from the SPARC database with deformed versions of two popular models of dark-matter halos, we collect some evidence that prolate dark-matter distributions improve by 5% or more the agreement with data for a wide fraction of the galaxies that we have examined. Moreover, the rotation curves of some galaxies seem to suggest the presence of string-like objects at their centers. If taken at face value, all these results would favor cold dark matter models (CDM) with respect to scenarios based on self-interacting dark matter (SiDM), modified gravity, or modified Newtonian dynamics (MOND).

Contents

1	Introduction	1
2	Deformed Dark–Matter Distributions	2
3	Fits of Observational Data	5
4	Conclusions	14

1 Introduction

Historically, the detection of flattened galaxy rotation curves [1] [2] was a key piece of evidence pointing to a dark–matter component in the Universe. The proposals to account for this phenomenon range from the so-called isothermal sphere DM distributions, which give rise to logarithmic gravitational potentials [3], to modifications of Newton’s laws at small accelerations, such as MOND (modified Newtonian dynamics) [4]. However, in most cases the rotation curves are not quite flat. Rather, they tend to have either slightly decreasing or slightly increasing profiles at large distances [5, 6], which suggests that their flattening is more likely the result of dynamical effects than of new physical laws.

In this paper we focus on a possible dynamical effect of this type, which apparently was not examined in detail before. Our message is that *standard physical laws can suffice to yield flattened rotation curves, at least within a given range of distances, in the presence of prolate dark–matter distributions*, via an effect whose origin would thus be purely geometric. Most importantly, the resulting masses of the halos lie, in most cases, within reasonable ranges, and flattened rotation curves could therefore reflect the presence of dark–matter bulges in galactic halos. Indeed, a number of galaxies and galaxy clusters, including Andromeda (M31) and the Milky Way, were estimated to have prolate dark halos, on the basis of kinematical data [7–9] or gravitational lensing [10, 11]. If dark matter density distributions, which for simplicity we still assume rotationally symmetric in the planes of galaxies, were elongated in the orthogonal directions, the resulting quasi-logarithmic potentials would yield near-constant rotation velocities within the two distance scales r_{xy} and r_z that characterize the extension of the dark matter profile within the galactic planes and away from them. Prolate halos were actually observed in simulations of collisionless CDM [12], and were conjectured

to result from either halo merging [13] or hierarchical structure formation, resulting in the collapse of matter along filaments rather than sheets [14]. However, DM self-interactions tend to favor rounder halo shapes [15], and the MOND framework can only mimic spherical or slightly oblate DM distributions [16]. As a result, ascertaining the actual presence of prolate halos would also provide additional evidence to discriminate among different scenarios, some of which also entail problematic features [17, 18].

In Section 2 we elaborate on analytical and numerical computations of gravitational potentials created by dark-matter distributions elongated away from galactic planes with deformed Burkert [19] and NFW profiles [20]. In Section 3, we make use of these deformed potentials to fit a fair number of rotation curves from the SPARC database [21]¹. We conclude in Section 4 with a summary of this work, some comments on its potential implications and a discussion of possible future lines of development.

2 Deformed Dark-Matter Distributions

Let us begin to explore the behavior of prolate dark-matter distributions in the simplest possible setting, the admittedly academic problem of a massive wire of finite length $2\ell_0$ through the center of a galaxy and orthogonal to its plane. Outside a spherical mass distribution, as is well known, the potential would have the standard $\frac{1}{r}$ behavior, while in this case

$$V(r) = G\mu \int_{-\ell_0}^{\ell_0} \frac{dz}{\sqrt{r^2 + z^2}} = G\mu \ln \left(\frac{\sqrt{\ell_0^2 + r^2} + \ell_0}{\sqrt{\ell_0^2 + r^2} - \ell_0} \right), \quad (2.1)$$

where μ is a mass per unit length and ℓ_0 is the length of the massive wire, which exhibits an interesting transition between a log-like behavior for $r \ll \ell_0$ and the standard $\frac{1}{r}$ behavior for $r \gg \ell_0$. In the former region the elongated mass distribution flattens the field lines in the galactic plane, mimicking a two-dimensional log-like behavior, before the standard monopole term finally dominates at larger distances. As a result, the corresponding velocity distribution,

$$v_{DM}^2(r) = -r \frac{\partial V(r)}{\partial r} = \frac{2G\mu\ell_0}{\sqrt{\ell_0^2 + r^2}}, \quad (2.2)$$

encodes a smooth transition between flat rotation curves and standard decaying profiles for $r \gg \ell_0$. Our aim in the following is to ascertain whether, and to which extent, bulges in the mass distributions of galaxies or wires of this type can account for flattened rotation curves. The potential interest in these considerations lies in the fact that they rest solely on standard laws of gravity, and in particular on its Newtonian limit, without the need for any infrared modifications.

¹A number of Groningen Ph.D. Theses were instrumental to build the catalogue. More details can be found in [21].

The Navarro-White-Frenk (NFW) [20] and Burkert [19] profiles,

$$\rho_{NFW}(r) = \frac{\rho_0 r_0^3}{r(r+r_0)^2}, \quad \rho_B(r) = \frac{\rho_0 r_0^3}{(r^2+r_0^2)(r+r_0)}, \quad (2.3)$$

are among the most popular spherically symmetric smooth distributions used for dark matter in galaxies. Making the simple replacement

$$r = \sqrt{x^2 + y^2 + z^2} \rightarrow \sqrt{x^2 + y^2 + qz^2}, \quad (2.4)$$

one can deform these spherical distributions into prolate ones for $q < 1$, or oblate ones for $q > 1$. The resulting contributions to the rotation velocity are determined by

$$-\frac{\partial V}{\partial r} = 2G \int_0^\infty dz \int_0^\infty dr' r' \rho(\sqrt{r'^2 + q^2 z^2}) \int_0^{2\pi} \frac{d\phi (r - r' \cos \phi)}{(r'^2 + r^2 + z^2 - 2rr' \cos \phi)^{3/2}}, \quad (2.5)$$

and performing the angular integral one can cast them in the form

$$v_{DM}^2(r) = -r \frac{\partial V}{\partial r} = \frac{2G}{r} \int_0^\infty dz \int_0^\infty dr' \frac{r' \rho(\sqrt{r'^2 + q^2 z^2})}{\sqrt{(r-r')^2 + z^2}} \left[F\left(\pi \mid -\frac{4rr'}{(r-r')^2 + z^2}\right) - \frac{r'^2 + z^2 - r^2}{(r+r')^2 + z^2} E\left(\pi \mid -\frac{4rr'}{(r-r')^2 + z^2}\right) \right], \quad (2.6)$$

where

$$F(\phi \mid x) = \int_0^\phi \frac{d\theta}{\sqrt{1-x^2 \sin^2 \theta}}, \quad E(\phi \mid x) = \int_0^\phi d\theta \sqrt{1-x^2 \sin^2 \theta} \quad (2.7)$$

are incomplete elliptic integrals of the first and second kind.

Eq. (2.6) is a complicated expression, which becomes however far simpler in the standard spherical limit ($q \rightarrow 1$), and also in the limit of infinite elongation away from the galactic plane ($q \rightarrow 0$). In the former case, the DM rotation velocity is determined by

$$v_{DM}^2(r) = \frac{4\pi G}{r} \int_0^r dr' r'^2 \rho(r'), \quad (2.8)$$

which results in

$$v_{NFW}^2(r) = \frac{4\pi G \rho_0 r_0^3}{r} \left[\ln\left(1 + \frac{r}{r_0}\right) - \frac{r}{r+r_0} \right], \quad (2.9)$$

$$v_B^2(r) = \frac{\pi G \rho_0 r_0^3}{r} \left[\ln\left(1 + \frac{r^2}{r_0^2}\right) + 2 \log\left(1 + \frac{r}{r_0}\right) - 2 \arctan\left(\frac{r}{r_0}\right) \right]$$

for the NFW and Burkert profiles. On the other hand, in the limit of infinite elongation the rotation velocity reflects the two-dimensional version of Gauss's theorem, so that

$$v_{DM}^2(r) = 4\pi G \int_0^r dr' r' \rho(r'), \quad (2.10)$$

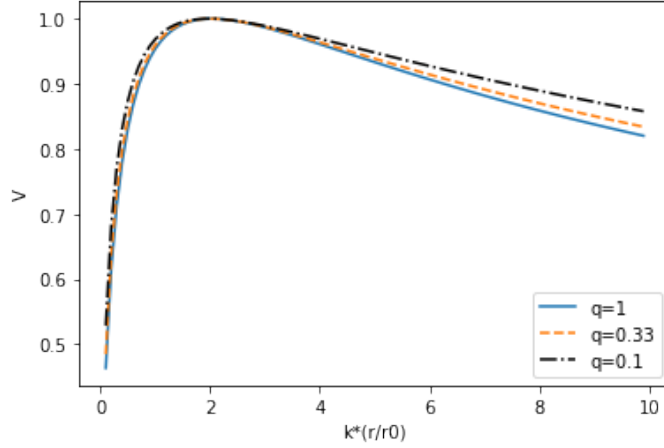


Figure 1. Dark-matter contributions to the rotation velocity for the NFW profile produced by a spherical halo (blue solid line), a prolate halo with a major-to-minor axis ratio 3 (orange dashed line), and a prolate halo with a major-to-minor axis ratio 10 (black dash-dotted line). The velocity is always normalized to unity at the peak, and the radius is normalized to $\frac{r_0}{k}$, with the coefficient k always chosen so that the peak lies at $k(\frac{r}{r_0}) = 2$. The actual value of r_0 depends on the galaxy.

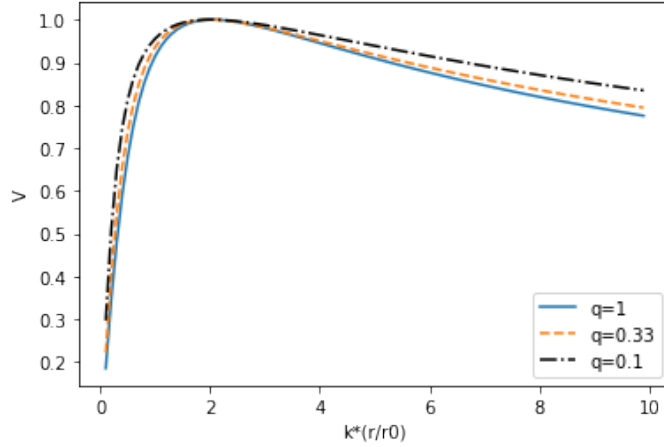


Figure 2. Dark-matter contributions to the rotation velocity for the Burkert profile produced by a spherical halo (blue solid line), a prolate halo with a major-to-minor axis ratio 3 (orange dashed line), and a prolate halo with a major-to-minor axis ratio 10 (black dash-dotted line). The velocity is always normalized to unity at the peak, and the radius is normalized to $\frac{r_0}{k}$, with the coefficient k always chosen so that the peak lies at $k(\frac{r}{r_0}) = 2$. The actual value of r_0 depends on the galaxy.

where $r = \sqrt{x^2 + y^2}$. In detail, for the deformed NFW and Burkert profiles

$$\begin{aligned}
 v_{NFW}^2(r) &= 4\pi G\rho_0 r_0^2 \frac{r}{r+r_0} , \\
 v_B^2(r) &= \pi G\rho_0 r_0^2 \left[\ln \left(1 + \frac{r^2}{r_0^2} \right) - 2 \log \left(1 + \frac{r}{r_0} \right) + 2 \arctan \left(\frac{r}{r_0} \right) \right] .
 \end{aligned}
 \tag{2.11}$$

From these expressions one can see that, if the density profile ρ has a characteristic radial scale r_0 beyond which it tends smoothly to zero, eventually $v_{NFW,B}^2 \propto r^{-1} \ln r$ in the spherical limit but $v_{NFW,B}^2 \propto \text{const}$ in the limit of infinite elongation. Even in the presence of smooth mass distributions, the effect we are after can therefore grant the emergence of flat rotation curves for distances scales $r_0 < r < q^{-1}r_0$, if $q < 1$. On the other hand, inside dark matter distributions one would observe growing rotation curves in both limits, with $v_{NFW}^2 \propto r$ and $v_B^2 \propto r^2$ for NFW and Burkert profiles. For generic bulged profiles the integrals must be computed numerically, and figs. 1 and 2 compare the results thus obtained with the spherical limits for the two cases of NFW and Burkert profiles. Our conclusion is therefore that, *for both NFW and Burkert profiles the dark-matter contributions to rotation velocities exhibit steep rises followed by shallow declines, and prolate halos yield steeper rises and shallower declines than the standard spherical ones.* This behavior complies to the picture that I have advocated at the beginning of this section, and we can now turn to a detailed comparison with the available data.

3 Fits of Observational Data

We have analyzed in detail 69 of the 175 galaxies of the SPARC database [21], performing a five-parameter fit with the function

$$v(r; Y_D, Y_B, \rho_0, r_0, q) = \sqrt{Y_D v_D^2(r) + Y_B v_B^2(r) + v_G(r)|v_G(r)| + v_{DM}^2(r, \rho_0, r_0, q)}. \quad (3.1)$$

The five parameters are the mass-to-light ratios Y_D and Y_B , bounded from below at 0.1, the two parameters ρ_0 and r_0 of the NFW and Burkert profiles of eq. (2.3), and finally the geometrical deformation parameter q . Notice that the absolute value is needed for the gas contribution, because it can become negative at smaller radii if the gas distribution is significantly depressed in the innermost regions, so that the gravitational pull from outwards is stronger than from inwards [21]. We were able to explore the resulting reduced χ^2 , minimized with respect to the other four parameters, within a significant range of values for q , and Tables 1 and 2 collect the values of q that yield the lowest value of χ^2 for each galaxy, together the corresponding percent improvements of the fit quality, which we quantify via

$$P_1 = 1 - \frac{\chi^2(q_{min})}{\chi^2(1)}, \quad (3.2)$$

where $\chi^2(1)$ denotes here the values for the spherical distributions.

Galaxy	$q_{min}(\text{NFW})$	$P_1, \%(\text{NFW})$	$P_2, \%(\text{NFW})$	$q_{min}(\text{Burk})$	$P_1, \%(\text{Burk})$	$P_2, \%(\text{Burk})$
NGC 1705	0.015	32.2	35	0.231	4.2	34
NGC 2841	0	6.2	19	0	20	40.4
NGC 2955	0.026	31.5	33.2	≥ 1	—	10
NGC 3198	≥ 1	—	—	0.107	53.4	18
NGC 3521	—	—	54.2	0	73.2	42
NGC 5005	—	—	38.6	0	0.2	45.7
NGC 5055	≥ 1	—	10.2	≥ 1	—	17
NGC 5371	0	68	68.3	0	84	84.3
NGC 5907	0	28.2	47.3	0	51.5	51.3
NGC 5985	0.63	0.2	—	0.1	30	25.8
NGC 6503	0.011	22.4	7	0.01	55	32.2
NGC 7331	0	8.2	5.7	0	29.4	41
NGC 7814	0	4.3	—	0	28.5	17
UGC 02953	0.1	1	25	0.023	18.6	40
UGC 06786	0.063	26.7	50	0.046	81	77.4
UGC 08699	0.01	1	10.3	0	10	30.5
UGC 09133	0	12	12.3	0	20.8	22
UGC 12506	≥ 1	—	5.2	0	77.5	69.4

Table 1: Some details on the galaxies, within the set of 69 that we have analyzed, which exhibit a preference for bulged shapes or string-like objects at their centers. In all these cases, the improvement factor (3.2) is larger than 10% for at least two of the four types of halos that we have explored. The left portion of the table concerns deformed NFW halos and spherical NFW halos supplemented with the $L \rightarrow \infty$ limit of the string-like contribution of eq. (2.1), while the right portion contains corresponding results for Burkert profiles.

Galaxy	$q_{min}(\text{NFW})$	$P_1, \%(\text{NFW})$	$P_2, \%(\text{NFW})$	$q_{min}(\text{Burk})$	$P_1, \%(\text{Burk})$	$P_2, \%(\text{Burk})$
DDO 161	≥ 1	—	—	≥ 1	—	35.1
DDO 168	—	—	—	≥ 1	—	—
ESO563-G021	—	—	—	≥ 1	—	—
F583-1	≥ 1	—	—	≥ 1	—	—
IC 2574	—	—	0.5	0	0.3	—
IC 4202	≥ 1	—	—	≥ 1	—	—
NGC 0024	—	—	—	≥ 1	—	—
NGC 0055	≥ 1	—	—	≥ 1	—	9.5
NGC 0100	—	—	0.1	0.346	2.6	—
NGC 0247	0	0.8	—	—	—	16
NGC 0289	≥ 1	—	—	0.073	1.4	3.1
NGC 0300	≥ 1	—	—	0	7.4	—
NGC 0891	≥ 1	—	—	≥ 1	—	—
NGC 1003	0	1.2	—	0	12.7	—
NGC 1090	≥ 1	—	—	0.5	6.4	1.1
NGC 2366	≥ 1	—	—	≥ 1	—	—
NGC 2403	0.35	0.6	—	0.037	6	8.2
NGC 2903	≥ 1	—	—	0.134	46.1	—
NGC 2976	—	—	—	≥ 1	—	—

NGC 3109	—	—	0.2	0.295	0.9	20
NGC 4013	—	—	0.6	0	0.8	6.5
NGC 4183	0	6.5	—	—	—	3.5
NGC 3741	≥ 1	—	—	0	8.7	—
NGC 4100	≥ 1	—	—	≥ 1	—	—
NGC 4217	≥ 1	—	—	≥ 1	—	—
NGC 4559	≥ 1	—	—	≥ 1	—	10
NGC 5033	≥ 1	—	—	≥ 1	—	—
NGC 5585	≥ 1	—	6.3	≥ 1	—	27.1
NGC 6015	0	17	—	≥ 1	—	7
NGC 6195	≥ 1	—	5.1	≥ 1	—	—
NGC 6946	≥ 1	—	—	0.388	0.1	7.8
NGC 7793	≥ 1	—	—	≥ 1	—	—
UGC 00128	0.37	0.4	—	≥ 1	—	51
UGC 02487	0	0.3	—	0	3	—
UGC 02916	≥ 1	—	—	≥ 1	—	0.3
UGC 03205	0	28	0.2	0	0.4	7
UGC 03546	≥ 1	—	—	≥ 1	—	—
UGC 03580	0.002	0.3	0.5	0	12.2	2.5
UGC 04278	—	—	0.1	≥ 1	—	1.2
UGC 05253	≥ 1	—	19.5	≥ 1	—	1.3
UGC 05721	≥ 1	—	—	≥ 1	—	1.7
UGC 05764	≥ 1	—	—	≥ 1	—	—
UGC 06787	—	—	—	0	0.04	1.2
UGC 07399	≥ 1	—	—	0	36.1	—
UGC 07524	≥ 1	—	—	≥ 1	—	6.3
UGC 08490	≥ 1	—	—	0.254	6	11.4
UGC 09037	≥ 1	—	—	0.23	7	—
UGC 11455	—	—	—	≥ 1	—	—
UGC 11820	≥ 1	—	—	0	9.3	—
UGC 11914	—	—	—	—	—	—
UGCA 444	—	—	0.2	0	0.2	—

Table 2: Some details on the galaxies, within the set of 69 that we have analyzed, with little or no preference for prolate shapes or string-like objects at their centers. In all these cases, the quality improvement factor (3.2) is less than 10% for at least three of the four types of halos that we have explored. The left portion of the table concerns deformed NFW halos and spherical NFW halos supplemented with the $L \rightarrow \infty$ limit of the string-like contribution of eq. (2.1), while the right portion contains corresponding results for Burkert profiles.

Our analysis shows that 22 of the 69 galaxies that we have examined favor prolate NFW profiles, while 37 of them favor them for the Burkert profile (Table 1). Somewhat surprisingly, however, in most of these cases the optimal value of q corresponds to large elongations, by a factor of 10 or more (corresponding to $q \leq 0.1$), and even larger values of $q < 1$ lead in general to better agreements with data than the ordinary spherically symmetric profiles with $q = 1$. This type of pattern can be clearly illustrated providing further details for the two

galaxies NGC 6503 (fig. 3 and 4) and NGC 2403 (fig. 5 and 6). Although the corrections are significant for the former and marginal for the latter, $\chi^2(q)$ is in both cases lower for $q < 1$ than for spherical dark-matter profiles, and increases monotonically for the oblate ones with $q > 1$. Moreover, the deformed halos result in rotation curves that are flatter at large distances, which yields a better agreement with the farthest available data points in fig. 5 and 6.

We left out galaxies whose characteristic scale r_0 , estimated in both limits $q \rightarrow 1$ and $q \rightarrow 0$, is larger than the rotation distances by an order of magnitude or more. Visually, this would result in monotonically increasing rotation curves without a peak, and in these situations one cannot discern whether or not the halos are prolate, since the corrections are negligibly small at radii much smaller than r_0 . Halos of this type are marked by dashes in the q_{min} columns of Tables 1 and 2.

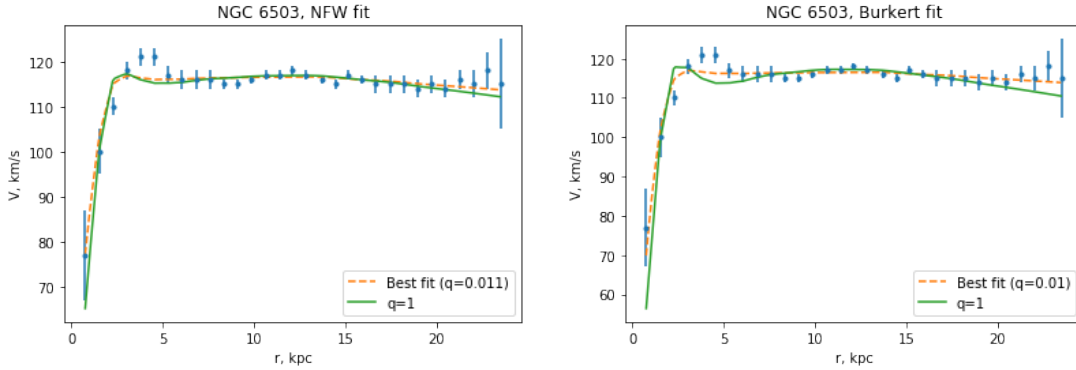


Figure 3. The rotation curve of NGC 6503, fitted by a spherical dark halo (green solid curve) and by a deformed halo (orange dashed curve). Left panel: NFW profile; right panel: Burkert profile.

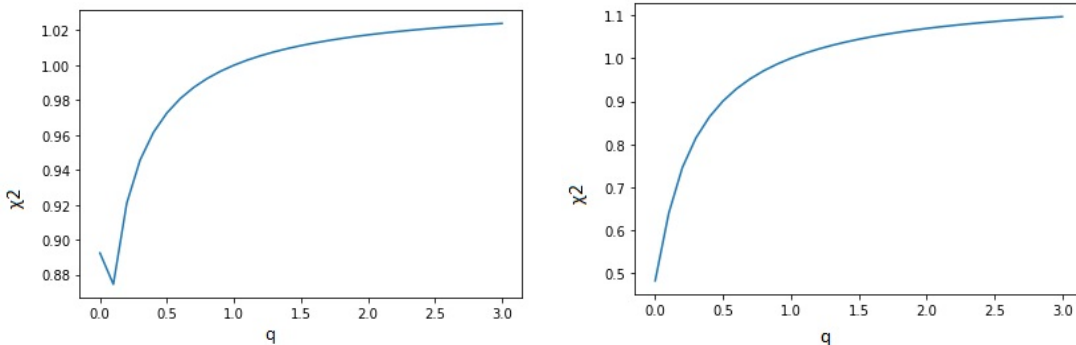


Figure 4. The χ^2 of the optimal fit as a function of the deformation parameter q for NGC 6503, normalized to 1 at $q = 1$. Left panel: deformed NFW profile; right panel: deformed Burkert profile.

There are also galaxies without prolate halos, where the effect that we are advocating

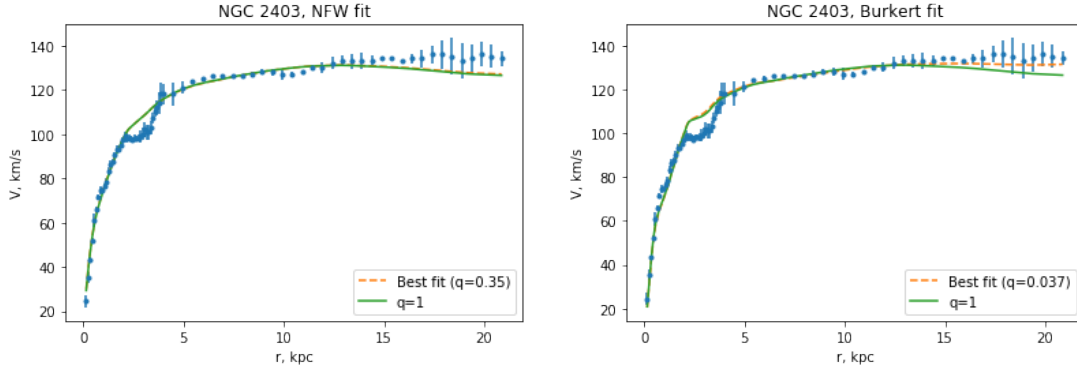


Figure 5. The rotation curve of NGC 2403, fitted by spherical dark halo (green solid curve) and by a deformed halo (orange dashed curve). Left panel: NFW profile; right panel: Burkert profile.

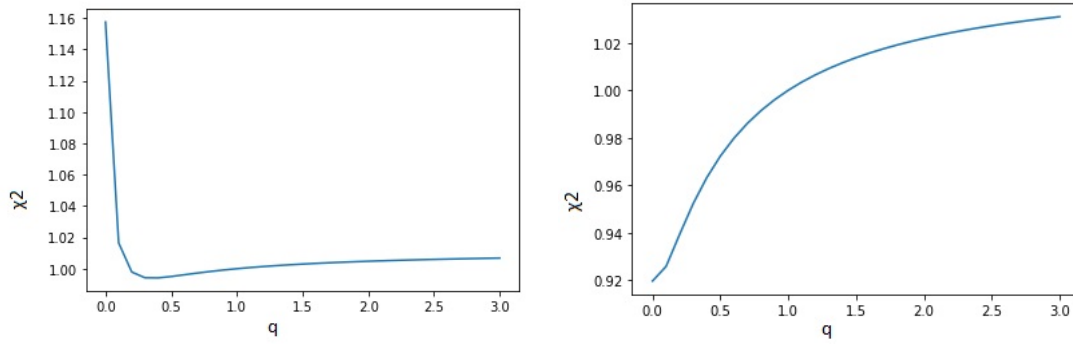


Figure 6. The χ^2 of optimal fit as a function of the deformation parameter q for NGC 2403, normalized to 1 at $q = 1$. Left panel: NFW profile; right panel: Burkert profile.

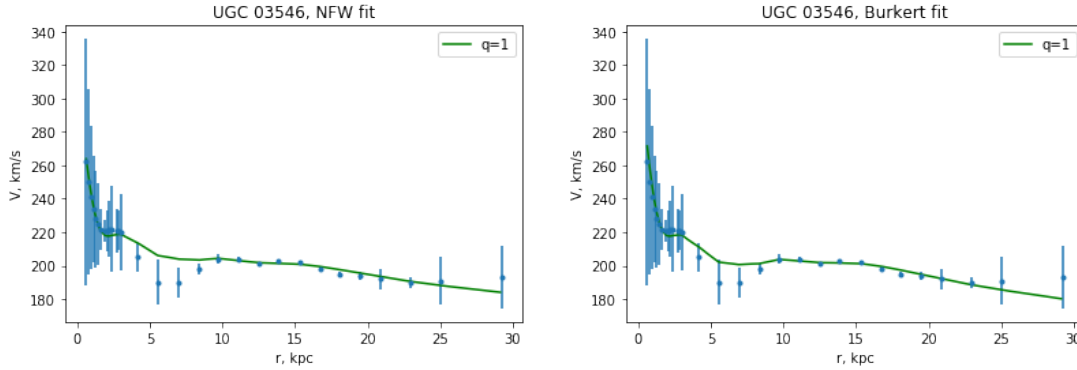


Figure 7. The rotation curve of UGC 03546, fitted by spherical dark halos (green solid curve). Left panel: NFW profile; right panel: Burkert profile.

appears irrelevant. This different type of pattern is well illustrated by the case of UGC 03546, whose $\chi^2(q)$ decreases monotonically from $q = 0$ to $q \geq 3$ (figs. 7 and 8). However, this result is again at odds with the modified gravity paradigm, which can only mimic spherical or

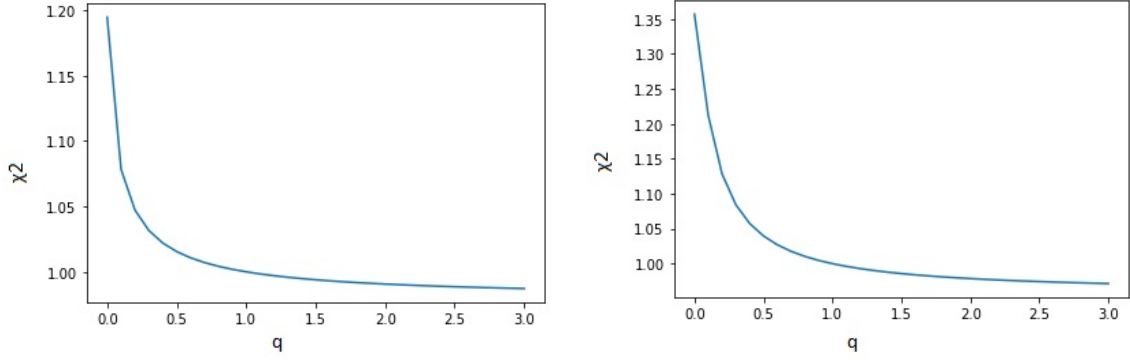


Figure 8. The χ^2 of optimal fit as a function of the deformation parameter q for UGC 03546, normalized to 1 at $q = 1$. Left panel: NFW profile, right panel: Burkert profile.

slightly oblate geometries.

In addition, we have computed the virial masses of the ellipsoidal halos, which are defined as

$$M = \int d^3r \rho(\vec{r}) = \frac{4\pi}{q} \int_0^{r_c} dr r^2 \rho(r). \quad (3.3)$$

Here we have defined r_c , in an admittedly arbitrary but reasonable manner, demanding that the average DM density within the ellipsoid be 200 times larger than the critical density of the Universe [22]:

$$\frac{M}{200 \left(\frac{4\pi\rho_c r_c^3}{3q} \right)} = \frac{\pi G}{25H^2 r_c^3} \int_0^{r_c} dr r^2 \rho(r) = 1. \quad (3.4)$$

For the NFW and Burkert profiles, the halo masses are

$$\begin{aligned} M_{NFW} &= \frac{4\pi\rho_0 r_0^3}{q} \left[\ln\left(1 + \frac{r_c}{r_0}\right) - \frac{r_c}{r_c + r_0} \right], \\ M_B &= \frac{\pi\rho_0 r_0^3}{q} \left[\ln\left(1 + \frac{r_c^2}{r_0^2}\right) + 2\ln\left(1 + \frac{r_c}{r_0}\right) - 2\arctan\left(\frac{r_c}{r_0}\right) \right]. \end{aligned} \quad (3.5)$$

A number of halos, as we have stressed, have best fits for values of q that are close to zero, which would result in diverging virial masses. For this reason we have introduced in this analysis a cutoff at $q = 0.1$. Nonetheless, for both NFW and Burkert profiles the scatter plots in fig. 9 show that galaxies with $q = 0.1$ are systematically more massive than galaxies with $q = 1$, and this result is in good agreement with numerical simulations [13, 14].

We have also examined another possible origin for the flattening of rotation curves, the presence of an infinitely thin, string-like object at the center of the galaxy. An object of this type would produce a logarithmic potential, adding a constant term v_s^2 in the squared rotation velocity and turning it into

$$v(r; Y_D, Y_B, \rho_0, r_0, q, v_s) = \sqrt{Y_D v_D^2(r) + Y_B v_B^2(r) + v_G(r)|v_G(r)| + v_{DM}^2(r, \rho_0, r_0, 1) + v_s^2}. \quad (3.6)$$

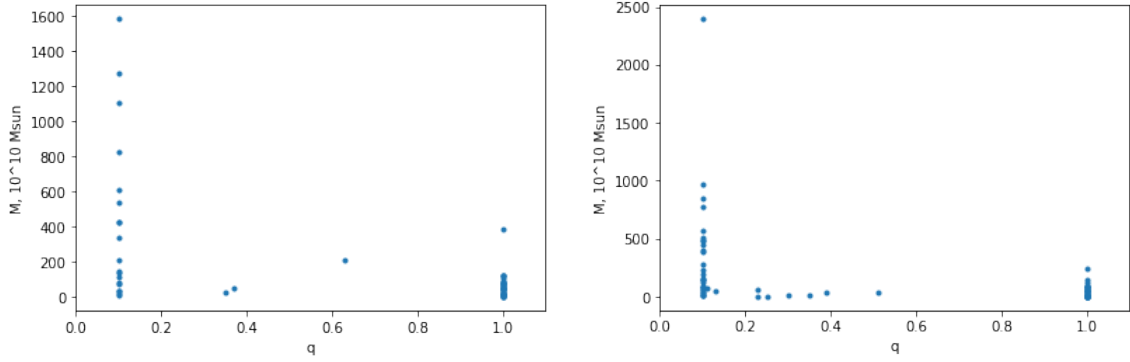


Figure 9. Scatter plots for the virial mass distributions of galaxies versus the corresponding distributions of q , which quantifies the extensions of their dark-matter halos away from galactic planes. As explained in the text, we have set a lower bound on q . Large virial masses are preferentially accompanied by bulged dark-matter halos. Left panel: NFW profiles; right panel: Burkert profiles.

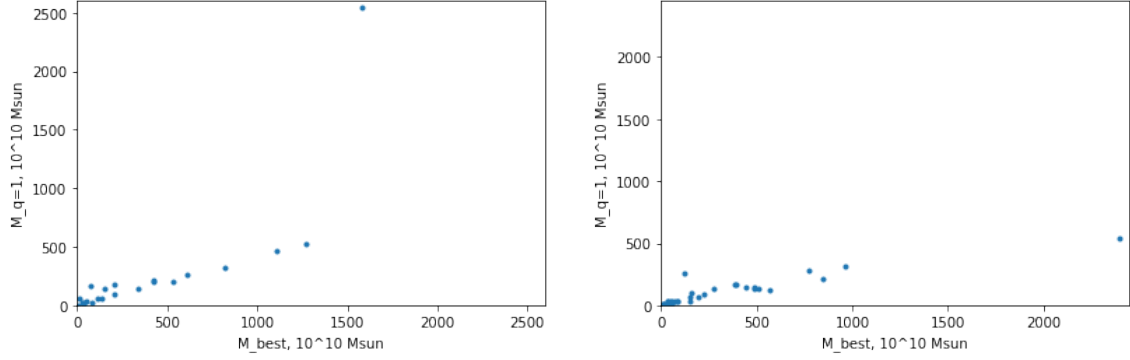


Figure 10. Scatter plots for the virial mass distributions of prolate halos versus the corresponding spherical virial masses with $q = 1$. For most galaxies that favor elongated halos, these feature masses a few times larger than those expected in the spherical case.

In this analysis we have confined our attention to galactic halos that, aside from this contribution, are spherically symmetric, since our intent was to clarify whether, and to which extent, the two phenomena are interchangeable, and in which cases one of them is clearly preferable. These results, for both for NFW and Burkert halos, are also included in Tables 1 and 2. The corresponding figure of merit is now

$$P_2 = 1 - \frac{\chi^2(v_{s,min})}{\chi^2(0)}, \quad (3.7)$$

where $\chi^2(0)$ denotes here the value for the spherical distribution without an additional string-like object at the center. Two examples where an additional string-like object appears preferable over halo bulges are the galaxies NGC 5371 and NGC 5907 (figs. 11 and 12). Fitting them with ellipsoidal halos leads indeed, in both cases, to preferred configurations with $q \rightarrow 0$ and $r_0 \rightarrow 0$, which also point to string-like dark halos.

A more realistic setup of this type ought to involve string-like objects of finite length, and thus with a finite total mass. This is the very setting that motivated the present investigation. Therefore, we have also attempted fits where, for the galaxies in Table 1, the constant v_s^2 is replaced with (2.2). The results for NFW and Burkert profiles are collected in Tables 3 and 4. Reassuringly, in most cases the addition of a finite string-like object does not increase significantly the total mass of the system. However, for a few galaxies it does lead to unphysical halos, with masses above $10^{14}M_\odot$.

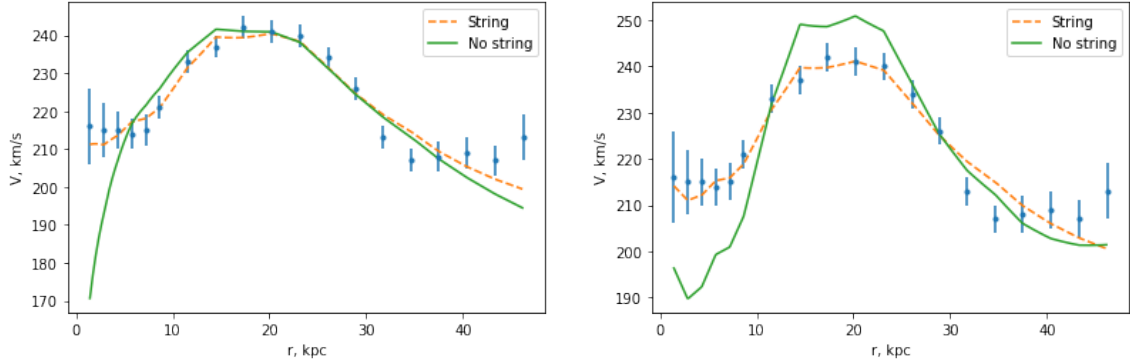


Figure 11. Rotation curves for the galaxy NGC 5371 with a string-like object at the origin (dashed orange line) and without one (solid green line). Notice the improvements, corresponding to values of P_2 of about 68% and 84%, which are obtained adding a string-like object the center. Left panel: NFW profile; right panel: Burkert profile.

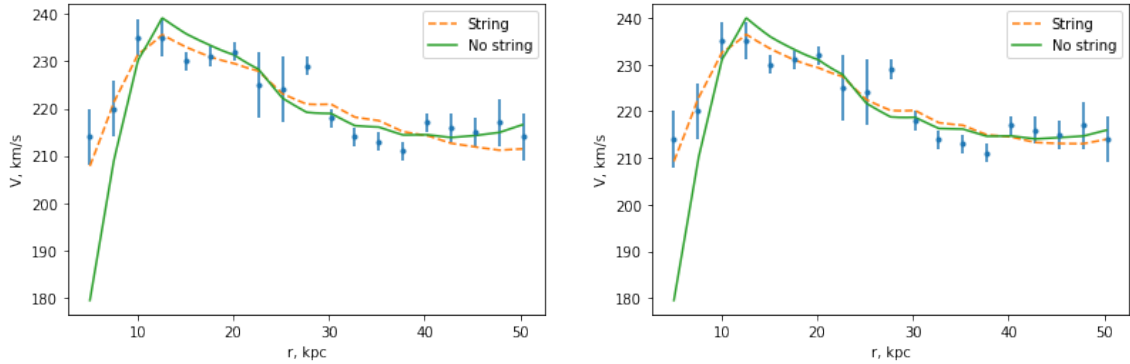


Figure 12. Rotation curves for the galaxy NGC 5907 with a string-like object at the origin (dashed orange line) and without one (solid green line). Notice the improvements, corresponding to values of P_2 of about 47% and 51%, which are obtained adding a string-like object the center. Left panel: NFW profile; right panel: Burkert profile.

Galaxy	$M_h/10^{10}M_\odot$ (no string)	$M_h/10^{10}M_\odot$ (string)	$M_s/10^{10}M_\odot$	L, kpc	$G\mu/c^2, 10^{-6}$	$P_2, \%$
NGC 1705	3	2.8	0.02	2	0.002	36
NGC 2955	140	111	6	25	0.06	92
NGC 3521	24795	201	13	50	0.07	54
NGC 5005	11714	1645	30	50	0.2	44
NGC 5055	67	51	13	100 (c)	0.03	11
NGC 5371	61	15	60	100 (c)	0.2	66
NGC 5907	2550	795	60	100 (c)	0.1	46
NGC 6503	18	19	0.3	5	0.02	8
NGC 7331	146	3228	11	14	0.2	21
UGC 02953	208	227	1	1	0.3	31
UGC 06786	99	52	100	200	0.1	50
UGC 08699	202	459	1.5	13	0.03	10
UGC 09133	200	0	320	333	0.2	13
UGC 12506	119	116	1.1	33	0.01	6

Table 3: Mass comparisons between galaxies fitted with only spherical NFW halos and with combinations of spherical NFW halos and string-like objects at the origin. The second column contains the virial masses of the halos when elongated objects are not present, the third column contains the virial masses of the halos with elongated objects, and finally the fourth column contains the total masses of the objects. In most cases, the total masses of the NFW halos and the objects is either smaller than the halo masses in absence of the objects, or exceed them by a factor not larger than 2–2.5. The exceptions are the galaxies NGC 7331 and NGC 2841, whose halo masses increase by more than an order of magnitude after adding the string. NGC 2841 is not shown in the table, since its halo mass becomes too large and approaches non-physical values beyond $10^{14}M_\odot$. The label 100(c) marks the cases where the optimal string length was beyond the cutoff at 100 kpc. Whenever we introduced the cutoff, the resulting improvement factor P_2 was slightly worse than for an infinite string, while in other cases strings of finite lengths led to better fits.

Should these elongated objects really exist, their precise nature remains unclear. An object of this type, supposedly located at the center of the Milky Way, was conjectured to be a cosmic string [23], and gravitational waves produced by cosmic strings were also suggested to be the origin of distortions in pulsar signals observed by the NANOGrav collaboration [24, 25]. In scenarios where cosmic strings and primordial black holes (PBHs) are both present in the early Universe, strings can attach themselves to PBHs and form networks. Assuming that the supermassive black holes at the centers of galaxies originate from PBHs, cosmic strings could indeed be present there [26], and the estimated values of the string tension $\frac{G\mu}{c^2}$, presented in Tables 3 and 4, are below the upper observational bound from the CMB, which is $3.7 * 10^{-6}$ [27]. Black-hole jets, or tidal streams of baryonic or dark matter might be alternative candidates [28]: for instance, NGC 5907 is known to host an extended stellar tidal stream [29, 30]. It remains to be seen whether its gravitational potential can yield the proper log-like behavior.

Galaxy	$M_h/10^{10}M_\odot$ (no string)	$M_h/10^{10}M_\odot$ (string)	$M_s/10^{10}M_\odot$	L, kpc	$G\mu/c^2, 10^{-6}$	$P_2, \%$
NGC 1705	2	2.8	0.03	2	0.005	27
NGC 2955	116	92	5	20	0.06	35
NGC 3198	35	31	4	100 (c)	0.01	16
NGC 3521	124	77	4	20	0.05	42
NGC 5005	208	51	62	100 (c)	0.2	46
NGC 5055	59	40	17	100 (c)	0.04	12
NGC 5985	180	90	60	100 (c)	0.2	22
NGC 6503	14	4	17	100 (c)	0.04	29
NGC 7331	14	790	17	20	0.3	44
UGC 02953	171	181	1.1	1	0.3	29
UGC 06786	97	30	66	100 (c)	0.2	74
UGC 08699	66	71	28	100 (c)	0.07	30
UGC 09133	168	23	153	167	0.2	22
UGC 12506	132	80	17	50	0.08	86

Table 4: Mass comparisons between galaxies fitted with only spherical Burkert halos and with combinations of spherical NFW halos and string-like objects at the origin. The second column contains the virial masses of the halos when elongated objects are not present, the third column contains the virial masses of the halos with elongated objects, and finally the fourth column contains the total masses of the objects. In most cases, the total masses of the Burkert halos and the objects is either smaller than the halo masses in absence of the objects, or exceeds them by a factor of no more than 2-2.5. The exceptions are the galaxies NGC 7331, NGC 2841, NGC 5371, NGC 5907, and NGC 7814 whose halo masses increase by more than an order of magnitude after the addition of the string. NGC 2841, NGC 5371, NGC 5907, and NGC 7814 are not shown in the table, since their halo masses become too large and approach non-physical values beyond $10^{14}M_\odot$. The label 100(c) marks the cases where the optimal string length was beyond the cutoff at 100 kpc. We had to introduce the cutoff, the resulting improvement factor P_2 is slightly worse than for an infinite string, while in other cases strings of finite lengths led to better fits.

4 Conclusions

In this paper we have elaborated on the idea that flattened rotation curves could reflect the elongation of dark matter halos away from galactic planes. As we have seen in Section 2, bulged dark-matter distributions can squeeze Newtonian field lines around galactic planes, giving rise to quasi-logarithmic potentials within a range of distances from the galactic center. This setting would be at variance with the standard picture, which ascribes flattened rotation curves to the dominant presence of dark matter in the outer regions of galactic planes.

In the first part of this work, after highlighting the phenomenon in its simplest instance, we have turned to the two popular NFW and Burkert density profiles, whose spherical versions are often used for fits of galaxy rotation curves. However, we have deformed these spherical profiles performing in their arguments the simple substitution in eq. (2.4), so that $q < 1$ corresponds to bulged dark-matter profiles, while $q > 1$ corresponds to dark-matter profiles that are squeezed around galactic planes. While admittedly arbitrary, this simple

deformation is arguably a suggestive departure from spherical profiles that grants a first comparison of our picture with data at the price of a single additional parameter. Armed with these ingredients, we have performed fits of 69 galaxy rotation curves from the SPARC sample with deformed NFW and Burkert profiles. We have thus discovered that, *for a sizable fraction of the galaxies that we have examined, elongated dark-matter halos are in better agreement with observations than spherical ones.* In addition, while the accumulation of data points around $q = 0.1$ in the scatter plots of fig. 9 reflects the cutoff that we have imposed for reasons detailed in the preceding section, it is fair to conclude, in our opinion, that prolate dark-matter halos tend to accompany larger DM distributions.

This work has clearly some limitations, which make its conclusions at best preliminary. Most notably, we have worked with simple deformations of two specific, if very popular, density profiles. Moreover, while confining the attention to bulges orthogonal to galactic planes appears natural, in view of the expected rotational motion of all matter, whether luminous or dark, ellipsoidal shapes are clearly an arbitrary choice. We can only justify it on grounds of simplicity, economy of parameters and variety of the scenarios that it can capture, which include infinitely long strings as limiting cases. However, we have also explored combinations of string-like objects, even of finite length, with standard spherical halos, whose neat properties, summarized in eqs. (2.1) and (2.2), provided the original motivation for this work. Lo and behold, the rationale behind our approach is spelled out in the discussion at the beginning of Section 2: our main motivation was to try and connect quasi-logarithmic potentials to the squeezing of field lines around galactic planes induced by generic dark-matter bulges, and *we have collected some evidence, exploring their rotation curves with deformed NFW or Burkert profiles, that several galaxies among the 69 that we have analyzed favor prolate halo shapes or, in some cases, the presence of string-like objects at their centers.* This result lends, in our opinion, some credence to the dynamical effect we were after, which would also forego the need for infrared modifications of gravity in this context. A puzzling and surprising feature of our findings, however, is that for many of the galaxies that we examined the preferred choice of q is about 0.1 or smaller, which would signal the presence of huge bulges. However, we have reached these conclusions exploring continuous families of profiles for different values of q , which include less pronounced bulges. All prolate choices yield, for these galaxies, better fits than spherical halos, and in certain cases the suggested departures from spherical profiles could be detectable, since they are of the order of 5-15% for $q \sim 0.5$. Observations of gravitational lensing indicate that some galaxies and galaxy clusters have prolate dark matter distributions [10, 11], and future work in these directions will be instrumental to reinforce or disprove our findings.

Dark-matter bulges in galaxies entail a potential difficulty, since they increase the amount of dark matter in comparison to spherical halos, as can be seen for instance in fig. 10. With NFW profiles a spherical dark-matter halo would correspond typically to about 10^{12}

solar masses, while our preferred bulges increase this estimate by about 30%. On the other hand, with Burkert profiles our preferred bulges would increase the estimate almost by a factor of 2.5. With about 10^{11} galaxies in the Universe, the overall increase in the dark-matter component due to bulges could be of order 10^{23} solar masses. While this is sizable amount, it is reassuringly still below the Planck estimate for Ω_c [31] by more than a factor of two.

If prolate halos were to prove a generally dominant feature, this would have some bearing on the controversy between the cold dark matter (CDM) paradigm, self-interacting dark matter (SiDM), and models of modified gravity or modified Newtonian dynamics (MOND). To wit, CDM simulations often produce elongated halos [12], while SiDM favors rounded halos [15], and MOND is only expected to imitate spherical or slightly oblate dark density distributions [16]. It is not clear to us at present whether a sharper evidence for prolate halos could also impinge on hybrid models, such as superfluid dark matter, which at finite temperatures is expected to yield both a MOND-like modification of gravity and a CDM-like matter component [32].

The galaxies that exhibit a significant preference for prolate shapes, especially when the indication obtains for both NFW and Burkert profiles, can be tested independently by other observations, and in particular by the detection of kinematic stellar groups [33, 34]. Here we have focused on deformed dark-matter halos, since the uncertainties on their actual distributions leave ample room to explore this option, but for example other investigations point to the presence of a peculiar elongated object at the center of the Milky Way, which was conjectured to be a cosmic string [23]. If similar phenomena were to occur in other galaxies, they would also help to produce logarithmic potentials, via effects along the lines of eq. (2.1). Finally, we are also aware that elongated objects comprising stars and gas clouds of luminous matter are frequently present near galaxy centers, in the vicinity of a black hole [28]. A key question would be to translate the presence of prolate features, or the lack thereof, into insights on the formation processes of the different types of galaxies that this type of analysis points to. The more refined galaxy surveys expected from the Euclid mission are likely to shed more light on these important issues [35].

Acknowledgments

I am grateful to S. McGaugh for clarifications on the SPARC database, and to Ivano Basile for discussions and help with Cython codes. I am very grateful to A. Sagnotti for suggesting to look into halo bulges away from galactic planes and to A. Ferrara for his detailed comments and suggestions on the manuscript. I am also grateful to DESY-Hamburg, where part of this work was done, for the kind hospitality extended to me. This work was supported in part by Scuola Normale Superiore, by INFN (IS CSN4-GSS-PI) and by the MIUR-PRIN contract

References

- [1] V. C. Rubin and W. Ford, Jr., *Astrophys. J.* **159** (1970) 379.
- [2] Y. Sofue and V. Rubin, *Ann. Rev. Astron. Astrophys.* **39** (2001) 137 [arXiv:astro-ph/0010594 [astro-ph]].
- [3] J. Binney and S. Tremaine, “Galactic Dynamics” (Princeton University Press, Princeton, 2008).
- [4] M. Milgrom, *Astrophys. J.* **270** (1983) 365.
- [5] M. Persic, P. Salucci and F. Stel, *Mon. Not. Roy. Astron. Soc.* **281** (1996) 27 [astro-ph/9506004].
- [6] P. Salucci, A. Lapi, C. Tonini, G. Gentile, I. Yegorova and U. Klein, *Mon. Not. Roy. Astron. Soc.* **378** (2007) 41 [astro-ph/0703115 [ASTRO-PH]].
- [7] K. Hayashi and M. Chiba, *Astrophys. J.* **789** (2014) 62 [arXiv:1405.4606 [astro-ph.GA]].
- [8] A. Bowden, N. Evans and A. Williams, *Mon. Not. Roy. Astron. Soc.* **460** (2016) 329 [arXiv:1604.06885 [astro-ph.GA]].
- [9] K. Hattori and M. Valluri, [arXiv:1909.03321 [astro-ph.GA]].
- [10] H. Hoekstra, H. K. C. Yee and M. D. Gladders, *Astrophys. J.* **606** (2004) 67. [arXiv:astro-ph/0306515 [astro-ph]].
- [11] M. Oguri, [arXiv:astro-ph/0408573 [astro-ph]].
- [12] J. Dubinski and R. G. Carlberg, *Astrophys. J.* **378** (1991) 496.
- [13] B. Allgood, R. A. Flores, J. R. Primack, A. V. Kravtsov, R. H. Wechsler, A. Faltenbacher and J. S. Bullock, *Mon. Not. Roy. Astron. Soc.* **367** (2006) 1781 [arXiv:astro-ph/0508497 [astro-ph]].
- [14] P. Bett, V. Eke, C. S. Frenk, A. Jenkins, J. Helly and J. Navarro, *Mon. Not. Roy. Astron. Soc.* **376** (2007) 215 [arXiv:astro-ph/0608607 [astro-ph]].
- [15] N. Yoshida, V. Springel, S. D. M. White and G. Tormen, *Astrophys. J. Lett.* **544** (2000) L87 [arXiv:astro-ph/0006134 [astro-ph]].
- [16] J. I. Read and B. Moore, *Mon. Not. Roy. Astron. Soc.* **361** (2005) 971 [astro-ph/0501273].
- [17] S. Boran, S. Desai, E. O. Kahya and R. P. Woodard, *Phys. Rev. D* **97** (2018) no.4, 041501 [arXiv:1710.06168 [astro-ph.HE]].
- [18] K. Zatrimeylov, *JCAP* **08** (2020), 024 [arXiv:2003.10410 [gr-qc]].
- [19] A. Burkert, *IAU Symp.* **171** (1996), 175 [arXiv:astro-ph/9504041 [astro-ph]].
- [20] J. F. Navarro, C. S. Frenk and S. D. M. White, *Astrophys. J.* **490** (1997) 493 [arXiv:astro-ph/9611107 [astro-ph]].
- [21] F. Lelli, S. S. McGaugh and J. M. Schombert, *Astron. J.* **152** (2016) 157 [arXiv:1606.09251 [astro-ph.GA]], and references therein.
- [22] M. J. White, *Astron. Astrophys.* **367** (2001) 27 [arXiv:astro-ph/0011495 [astro-ph]].

- [23] M.R. Morris, J.-H. Zhao and W.M. Goss, *Astrophys. J. Lett.* **850** (2017) L23.
- [24] S. Blasi, V. Brdar and K. Schmitz, [arXiv:2009.06607 [astro-ph.CO]].
- [25] Z. Arzoumanian *et al.* [NANOGrav], [arXiv:2009.04496 [astro-ph.HE]].
- [26] A. Vilenkin, Y. Levin and A. Gruzinov, *JCAP* **11** (2018) 008 [arXiv:1808.00670 [astro-ph.CO]].
- [27] E. Jeong and G. F. Smoot, *Astrophys. J.* **624** (2005), 21-27 [arXiv:astro-ph/0406432 [astro-ph]].
- [28] J. Craig Wheeler, “Cosmic Catastrophes: Exploding Stars, Black Holes, and Mapping the Universe” (Cambridge Univ. Press, Cambridge, 2007).
- [29] D. Martinez-Delgado, J. Penarrubia, R. J. Gabany, I. Trujillo, S. R. Majewski and M. Pohlen, *Astrophys. J.* **689** (2008) 184 [arXiv:0805.1137 [astro-ph]].
- [30] P. van Dokkum, C. Gilhuly, A. Bonaca, A. Merritt, S. Danieli, D. Lokhorst, R. Abraham, C. Conroy, J. P. Greco, [arXiv:1906.11260 [astro-ph]].
- [31] N. Aghanim *et al.* [Planck], *Astron. Astrophys.* **641** (2020) A6 [arXiv:1807.06209 [astro-ph.CO]].
- [32] L. Berezhiani and J. Khoury, *Phys. Rev. D* **92** (2015) 103510 [arXiv:1507.01019 [astro-ph.CO]].
- [33] A. Rojas-Nino, O. Valenzuela, B. Pichardo and L. A. Aguilar, *Astrophys. J. Lett.* **757** (2012) L28 [arXiv:1112.4510 [astro-ph.GA]].
- [34] A. Rojas-Niño, L. A. Martínez-Medina, B. Pichardo and O. Valenzuela, *Astrophys. J.* **805** (2015) 29 [arXiv:1503.05861 [astro-ph.GA]].
- [35] R. Laureijs *et al.* [EUCLID], [arXiv:1110.3193 [astro-ph.CO]].